Late Pleistocene age and archaeological context for the hominin calvaria from GvJm-22 (Lukenya Hill, Kenya)

Christian A. Tryon[a,1], Isabelle Crevecoeur[b], J. Tyler Faith[c], Ravid Ekshtain[a], Joelle Nivens[d], David Patterson[e], Emma N. Mbua[f], and Fred Spoor[g,h]

[a]Department of Anthropology, Harvard University, Cambridge, MA 02138; [b]Unité Mixte de Recherche 5199, de la Préhistoire à l'Actuel: Culture, Environnement, et Anthropologie, Centre National de la Recherche Scientifique, Université de Bordeaux, 33615 Talence, France; [c]Archaeology Program, School of Social Science, University of Queensland, Brisbane, QLD 4072, Australia; [d]Department of Anthropology, New York University, New York, NY 10003; [e]Center for the Advanced Study of Hominid Paleobiology, Department of Anthropology, The George Washington University, Washington, DC 20052; [f]National Museums of Kenya, Nairobi, Kenya 00100; [g]Department of Human Evolution, Max Planck Institute for Evolutionary Anthropology, D-04103, Leipzig, Germany; and [h]Department of Cell and Developmental Biology, University College London, WC1E 6BT London, United Kingdom

Edited by Erik Trinkaus, Washington University, St. Louis, MO, and approved January 16, 2015 (received for review September 19, 2014)

Kenya National Museums Lukenya Hill Hominid 1 (KNM-LH 1) is a *Homo sapiens* partial calvaria from site GvJm-22 at Lukenya Hill, Kenya, associated with Later Stone Age (LSA) archaeological deposits. KNM-LH 1 is securely dated to the Late Pleistocene, and samples a time and region important for understanding the origins of modern human diversity. A revised chronology based on 26 accelerator mass spectrometry radiocarbon dates on ostrich eggshells indicates an age range of 23,576–22,887 y B.P. for KNM-LH 1, confirming prior attribution to the Last Glacial Maximum. Additional dates extend the maximum age for archaeological deposits at GvJm-22 to >46,000 y B.P. (>46 kya). These dates are consistent with new analyses identifying both Middle Stone Age and LSA lithic technologies at the site, making GvJm-22 a rare eastern African record of major human behavioral shifts during the Late Pleistocene. Comparative morphometric analyses of the KNM-LH 1 cranium document the temporal and spatial complexity of early modern human morphological variability. Features of cranial shape distinguish KNM-LH 1 and other Middle and Late Pleistocene African fossils from crania of recent Africans and samples from Holocene LSA and European Upper Paleolithic sites.

Middle Stone Age | Later Stone Age | ostrich eggshell | *Homo sapiens* | modern human origins

For Late Pleistocene African populations of modern humans, the constellation of behavioral changes encapsulated in the transition from the Middle Stone Age (MSA) to the Later Stone Age (LSA) ~70–20 kya represents a series of some of the most pronounced changes in the archaeological record before the adoption of domesticated animals and plants and the use of ceramics for cooking and storage. It is among LSA sites that the strongest parallels with ethnographic and historic foragers are observed. Typical archaeological signatures include lithic technologies focused on the production of microliths (small flakes, blades, and bladelets with one edge blunted or "backed") from bipolar, single-, and opposed-platform cores; an increased use of ground-stone tools; and implements made of wood and bone. These new technologies occur with the appearance of material correlates of social identity and networks of long-distance exchange, including ostrich eggshell (OES) beads, ochre, and nonlocal stone raw material, as well as increased dietary breadth, all consistent with larger, more dense, or more interconnected populations (1–9).

This same interval of ~70–20 kya witnessed a number of human dispersals across Africa, with eastern Africa host to one or more candidate populations for the expansion of *Homo sapiens* out of Africa (10–15). However, the eastern African hominin fossil record for this interval is extremely sparse and poorly dated, and it consists largely of isolated teeth or highly fragmentary crania and postcrania (16–18). Here, we reassess the age and context of the Kenya National Museums Lukenya Hill Hominid 1 (KNM-LH 1) partial calvaria from site GvJm-22 at Lukenya Hill, Kenya, the only eastern African fossil hominin from a Last Glacial Maximum [LGM; 19–26.4 kya (19)] LSA archaeological context. We construct a revised accelerator mass spectrometry (AMS) radiocarbon chronology built on 26 new dates on OES fragments. The revised chronology confirms the LGM age of KNM-LH 1 and expands the maximum age of the site to beyond the limits of the radiocarbon method. Increased radiometric age is consistent with new technological analyses that demonstrate previously unrecognized MSA elements that indicate assemblages spanning the MSA/LSA transition from deposits underlying KNM-LH 1. Morphometric analyses using a robust comparative dataset demonstrate the variability among African Late Pleistocene hominins, including candidate populations for out-of-Africa dispersals. They indicate that KNM-LH 1 is distinct from (*i*) modern Africans, (*ii*) *H. sapiens* from Holocene LSA sites, and (*iii*) European Upper Paleolithic modern humans, suggesting that it may sample a now extinct lineage.

GvJm-22: Site Setting and Excavation History

GvJm-22 is a one of a number of rock shelters on the ~16-km^2 inselberg of Precambrian gneiss known as Lukenya Hill (−1.48°, 37.0°) that rises ~100–200 m above the grasslands of Kenya's Athi-Kapiti Plain (Fig. S1). The rock shelter overlooks the historic migration path of large herds of blue wildebeest (*Connochaetes*

Significance

Modern human (*Homo sapiens*) fossils from eastern African archaeological contexts from ~70,000–20,000 years ago are rare, limiting our ability to understand the relationship between biological and behavioral change during a time and place characterized by major human demographic shifts, including dispersals. Our chronological, archaeological, and human paleontological analyses of the GvJm-22 rock shelter and Kenya National Museums Lukenya Hill Hominid 1 partial calvaria constrain the age of major behavioral changes among African foragers (the shift to Later Stone Age technologies) and demonstrate the morphological distinctness of Late Pleistocene African hominins from African Holocene or Late Pleistocene Eurasian hominins, complicating the history of modern human diversity.

Author contributions: C.A.T., I.C., and J.T.F. designed research; C.A.T., I.C., J.T.F., R.E., J.N., D.P., E.N.M., and F.S. performed research; C.A.T., I.C., J.T.F., and R.E. analyzed data; and C.A.T. and I.C. wrote the paper.

The authors declare no conflict of interest.

This article is a PNAS Direct Submission.

Freely available online through the PNAS open access option.

[1]To whom correspondence should be addressed. Email: christiantryon@fas.harvard.edu.

This article contains supporting information online at www.pnas.org/lookup/suppl/doi:10.1073/pnas.1417909112/-/DCSupplemental.

taurinus), Burchell's zebra (*Equus quagga burchellii*), hartebeest (*Alcelaphus buselaphus*), and impala (*Aepyceros melampus*) (20, 21). R. M. Gramly discovered the site and, from 1970 to 1973, excavated 21.75 m^2 to ≤250 cm below surface (cmbs), uncovering >50,000 stone artifacts and >3,000 well-preserved identified faunal remains, including a partial calvaria of *H. sapiens* (KNM-LH 1), the latter found at a depth of 138–140 cmbs in the initial test pit (Fig. S2). Fossils and artifacts occur within variably $CaCO_3$-cemented tan and gray sandy silts likely deposited by bedrock dissolution, slope wash, and aeolian processes; exfoliated slabs from the inselberg increase with depth (20, 22, 23). Artifact typology, the degree of fossilization of the fauna, and conventional radiocarbon dates on charcoal and bone collagen from the 1970s (Table 1) indicate that four Pastoral Neolithic and LSA archaeological assemblages from 0–110 cmbs date to the Holocene, separated by an unconformity from two Pleistocene assemblages, termed occurrence E (120–150 cmbs) and occurrence F (170–205 cmbs) (20, 25). The Pleistocene occurrence E and F lithic assemblages are characterized by the production of small (≤3 cm) flakes, blades, and bladelets retouched primarily into scrapers and backed pieces, and have been attributed to the LSA (20, 22, 23, 26). The faunal assemblages from both occurrences indicate a dry, grassy, savanna environment. They are dominated by the extinct alcelaphine bovid *Damaliscus hypsodon*, with arid-adapted taxa, such as Grevy's zebra (*Equus grevyi*) and oryx (*Oryx beisa*), found well outside their historic ranges (21, 27, 28). Our analysis of the identified microfauna (number of identified specimens = 9) revises Gramly's analysis (20) and indicates a semiarid savanna environment (*Gerbilliscus* sp., *Tachyoryctes cf. splendens*, and *Pedetes* sp., as well as *Crocidura* sp.), with the Vlei rat (*Otomys* sp.) and cane rat (*Thryonomys* sp.) indicating wetter habitats likely at or near the spring seeps that are still found near GvJm-22.

Gramly and Rightmire (29) report two radiocarbon dates on bones bracketing KNM-LH 1 (from samples at 135–140 cmbs and 140–145 cmbs), with fluorine and nitrogen values of KNM-LH 1 and the dated bones indicating a shared depositional history and an age between 17,670 ± 800 ^{14}C y B.P. and 17,700 ± 760 ^{14}C y B.P. However, the ages of KNM-LH 1 and the GvJm-22 sequence are usually considered unreliable because of the stratigraphically inverted ages of samples underlying KNM-LH 1 (Table 1) and skepticism about older radiocarbon dates on bone, particularly from the tropics (30–32). Early collagen pretreatment techniques yielded "collagen" where, in fact, none was present (as shown by later reanalysis with improved techniques)

Table 1. Radiocarbon dates from GvJm-22

Date, ^{14}C y B.P.	Calibrated age,* y B.P.	Material†	Trench	Occurrence	Depth, cmbs	Laboratory no.
1,330 ± 100	1,234 ± 104	Charcoal (twig)	Balk	A	45–50	N-1076
1,510 ± 50	1,413 ± 61	Bone collagen	Balk	A	45–50	UCLA-1709D
2,250 ± 50	2,245 ± 62	Bone collagen	Balk	C	70–75	UCLA-1709C
17,670 ± 800	21,461 ± 977	Bone collagen	Balk	E	135–140	UCLA-1709A
17,700 ± 760	21,483 ± 926	Bone collagen	Balk	E	140–145	UCLA-1709B
3,526 ± 27	3,794 ± 49	OES	A	D/E	110–120	UBA-24889
13,008 ± 68	15,560 ± 137	OES	A	E	120–130	UBA-24884
12,752 ± 59	15,193 ± 100	OES	A	E	120–130	UBA-24885
12,854 ± 63	15,350 ± 122	OES	A	E	120–130	UBA-24886
12,953 ± 60	15,486 ± 124	OES	A	E	140–150	UBA-24881
15,391 ± 95	18,656 ± 101	OES	A	E	140–150	UBA-24883
18,056 ± 96	21,884 ± 152	OES	A	E	140–150	UBA-24882
13,045 ± 67‡	15,615 ± 139	OES	A	E/F	160–170	UBA-24891
21,803 ± 142	26,048 ± 142	OES	A	F	190-breccia	UBA-24890
4,116 ± 32	4,662 ± 87	OES	B	E	120–130	UBA-24877
3,2967 ± 518	37,213 ± 681	OES	B	E	130–140	UBA-24880
4,250 ± 32	4,814 ± 52	OES	B	E/F	150–160	UBA-24879
4,049 ± 34	4,533 ± 84	OES	B	E/F	160–170	UBA-24887
27,915 ± 287	31,824 ± 385	OES	B	F	170–180	UBA-24878
5,960 ± 35	6,793 ± 50	OES	C	D	105–110	UBA-24888
15,320 ± 450	18,609 ± 520	Bone collagen	C + balk	F	180–185	GX-3699
13,730 ± 430	16,628 ± 603	Bone collagen	C + balk	F	190–195	GX-3698
9,910 ± 300	11,487 ± 482	Bone collagen	C + balk	F	190–195	HEL-535
4,448 ± 32	5,103 ± 109	OES	Test pit	E	120–130	UBA-23927
12,884 ± 59	15,393 ± 120	OES	Test pit	E	130–140	UBA-23928
19,666 ± 120	23,691 ± 167	OES	Test pit	E	130–140	UBA-23929
19,594 ± 119	23,607 ± 176	OES	Test pit	E	130–140	UBA-23930
19,794 ± 127	23,826 ± 167	OES	Test pit	E	130–140	UBA-23931
19,568 ± 119	23,574 ± 179	OES	Test pit	E	140–150	UBA-23933
28,041 ± 320§	31,985 ± 431	OES	Test pit	E	140–150	UBA-23934
28,230 ± 380§	32,210 ± 502	OES	Test pit	E	140–150	AA102890
33,308 ± 612¶	37,571 ± 768	OES	Test pit	E	140–150	UBA-23935
33,410 ± 570¶	37,665 ± 729	OES	Test pit	E	140–150	AA102889
46,710 ± 3,852	N.A.	OES	Test pit	E	140–150	UBA-23932

Radiocarbon dates (^{14}C y B.P.) are reported as mean and 1 standard deviation. Laboratory codes: AA, University of Arizona; GX, Geochron Laboratories; HEL, National Museum of Finland (Helsinki); N, Nishina Memorial; UBA, Queen's University Belfast; UCLA, University of California Los Angeles. N.A., not applicable.

*Ages were calibrated using IntCal13 (24) and reported at the 95% confidence interval.

†OES dates from GvJm-22 are reported here for the first time; others are from Gramly (20, 25).

‡Gray-black color indicates that the sample is burnt.

§Multiple analyses of the same specimen by different laboratories.

¶Multiple analyses of the same specimen by different laboratories.

or failed to remove contaminating modern carbon fully, strongly biasing dates older than ∼15 kya (33). The dates bracketing KNM-LH 1 used the Longin technique of collagen extraction (34), a modified form of which is still used today, whereas unknown methods were used to generate the lower, stratigraphically inverted dates.

A Revised Radiocarbon Chronology

A revised chronology for the GvJm-22 sequence is provided by 26 AMS radiocarbon dates on the carbonate fraction of unmodified OES fragments. OES is reliably dated by the AMS radiocarbon method, and dating OES is appropriate for the 1970–1973 collections housed at the National Museums of Kenya (NMK) because the material is resistant to diagenetic contamination and does not degrade with storage time like charcoal (2, 35–38). Sample preparation was similar to the procedures of Janz et al. (37) and incorporated a strong preanalysis acid etch designed to remove outer surfaces and any associated contamination. To measure reliability further, two OES samples were split and sent to different radiocarbon dating laboratories (University of Arizona and Queen's University Belfast), yielding statistically indistinguishable results for both samples. All dates are calibrated using the IntCal13 calibration curve (24) and are summarized in Table 1.

The new dates confirm an unconformity of ∼9,000 y at ∼120 cmbs separating the Holocene from the underlying Pleistocene deposits. This unconformity may be due to erosion or reduced sedimentation with increased vegetation and greater moisture availability during the Holocene. OES fragments from the Pleistocene strata were dated from across the site (Gramly's test pit; trenches A, B, and C; and remnant sediment balks; Fig. S2). These results (*i*) expand the age range of occurrence E to ∼15 to >46 kya; (*ii*) confirm Gramly's hypothesis (20) of postdepositional mixing in trench B; and (*iii*) suggest that Gramly's 5- to 10-cm-thick horizontal excavation levels cross-cut sedimentary deposits that dip ∼2° westward, with an age offset of ∼7,000 to 10,000 y between layers at equivalent depths in trench A and the adjacent test pit (Table 1 and Fig. S2).

We developed a Bayesian age model (39) for the KNM-LH 1 cranium (found at 138–140 cmbs) using only dates from the test pit ($n = 11$) in which it was originally found. OxCal 4.2 software was used to combine dates for samples with replicate analyses from multiple laboratories and to develop a bounded sequence of dates and phases (groups of dates from the same 10-cm-thick excavation level). The KNM-LH 1 hominin lies near the boundary of two excavated levels (130–140 cmbs and 140–150 cmbs). Both levels have dated samples that are substantially younger (∼9,000–15,000 y) than the other samples from the same 10-cm interval (UBA-23928 and UBA-23933; Table 1). We modeled these samples as younger than the remaining samples within their respective 10-cm-thick excavation level, assuming that their younger age resulted from increased stratigraphic height and proximity to the overlying 10-cm-thick excavation unit. The modeled results indicate an age range of 23,576–22,887 calibrated (cal) y B.P. for the KNM-LH 1 cranium. This age is very close to the ages of 21,461 ± 977 and 21,483 ± 926 cal y B.P. for the conventional radiocarbon dates on bone fragments from 135–140 cmbs and 140–145 cmbs originally reported by Gramly and Rightmire (29).

MSA Archaeology at GvJm-22

Our reanalysis of the archaeological deposits below occurrence E and the KNM-LH 1 partial calvaria suggests assemblages that span the MSA/LSA transition at GvJm-22. The sequence is characterized by the progressive shift in emphasis from flake production by Levallois methods to blade and bladelet manufacture from single and opposed platform cores and an increased use of backed pieces (microliths) at the expense of points and scrapers. The shift to LSA technology is seen in other artifacts as well. Large grindstones that show repeated, heavy use for grinding appear only in occurrence E, with the largest being fragmented but 154 mm in maximum dimension and weighing 1.1 kg, with 52-mm-wide and 73-mm-wide depressions on either side, producing an hourglass-shaped profile along the broken edge similar to ethnographic examples used for processing ochre, cartilage, seeds, fibrous tubers, or vegetables (40, 41). Ochre is present in small amounts (5.2 ± 4.4 g per 10-cm interval) throughout the sequence (from 30–225 cmbs), with a single piece with wear facets at 185–190 cmbs. Finished and unfinished OES beads ($n = 7$ from 120–160 cmbs) appear at 150–160 cmbs, at and immediately below the occurrence E interface.

We examined the cores found in strata below occurrence E, including occurrence F as defined by Gramly (20) at 170–205 cmbs, as well as an interval between occurrences E and F (160–170 cmbs) and the lowermost deposits (210–250 cmbs), which Gramly referred to as occurrence G in his unpublished notes (Table S1). Data from neither 160–170 cmbs nor occurrence G have been reported previously. Levallois cores form 10–33% of the studied sample ($n = 207$) from below occurrence E. Our understanding of the Levallois concept follows the definition of Boëda (42). Most of the GvJm-22 Levallois cores were originally identified by Gramly (20) as "disk-like" cores, and many are consistent with what Yellen et al. (43) term "micro-Levallois" and "Aduma" cores. The GvJm-22 Levallois cores show primarily centripetal and bidirectional patterns of flake removal from the upper surface and near-exclusive use of recurrent methods of flake production immediately before discard (Fig. 1); *éclats débordants* ($n = 3$) further indicate on-site knapping and Levallois core edge maintenance during reduction. Levallois flakes are, on average, small ($n = 23$, 29.8 ± 6.2 mm) but significantly larger ($t = 2.72$, df = 43, $P = 0.009$) than Levallois cores ($n = 54$, 25.4 ± 6.8 mm), although the scale of the difference (∼5 mm) is quite small in practical terms. The slight size difference between Levallois cores and Levallois flakes at discard suggests short operational chains, particularly for cores of chert ($n = 31$, 25.1 ± 3.9 mm) and obsidian ($n = 12$, 20.41 ± 3.9 mm), the most common raw materials among Levallois cores. Both chert and obsidian are locally available only as small (∼5 cm) clasts and lapilli (23). Quartz Levallois core size ($n = 10$, 32.5 ± 10.8 mm) is significantly larger

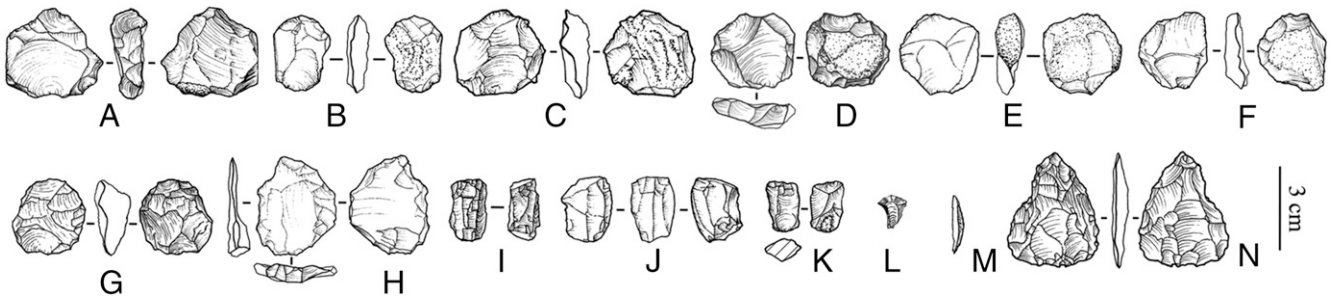

Fig. 1. Artifacts from strata beneath occurrence E of the 1970–1973 excavations at GvJm-22. Levallois cores (*A*–*G*), Levallois flake (*H*), bladelet cores (*I* and *J*), bipolar core (*K*), "fan" scraper (*L*), backed piece (*M*, microlith), and bifacial point (*N*). Artifacts *E*, *F*, *J*, and *N* are from the occurrence E/F interface (160–170 cmbs), artifact *A* is from occurrence G, and the remainder are from occurrence F. All are made chert, except for *G* (quartz) and *K* and *N* (obsidian).

($F = 12.05$, df = 2, $P < 0.001$) and more variable, likely reflecting the immediate availability of this material from veins within the Lukenya Hill inselberg.

Levallois cores and flakes co-occur with a number of other approaches to the production of small blanks (Fig. 1). Non-Levallois cores are also small ($n = 154$, 26.5 ± 8.9 mm) and do not differ significantly in size from the Levallois cores ($t = 1.01$, $P = 0.31$) or in the relative abundance of the use of chert, quartz, or obsidian ($\chi^2 = 4.068$, df = 2, $P = 0.13$). These other flake, blade, and bladelet production methods form the technological substrate throughout the Pleistocene sequence at GvJm-22, and the difference between occurrence E and strata beneath it lies in the increased frequency of platform cores for blade and bladelet production, increased use of the bipolar method, and the abandonment of Levallois and other centripetal approaches over time, differences that are significant ($\chi^2 = 232.45$, df = 6, $P < 0.001$).

A similar gradation is found among the retouched tools, with differences between occurrence E and the strata below being primarily a difference of quantity rather than kind, with backed pieces and scrapers (Fig. 1) present at ≤195 cmbs. Based on counts from Gramly (20) and our metric data, backed pieces form the dominant retouched tool in occurrence E (measured sample: $n = 128$, 21.3 ± 4.7 mm) but do not differ in size from those backed pieces in occurrence F ($n = 15$, 23.8 ± 7 mm; $t = 1.35$, $P = 0.20$), where they are more rare. Scrapers are the most abundant retouched tool in occurrence F, and the difference between the archaeological occurrences of backed pieces and scrapers is significant ($\chi^2 = 158.06$, df = 1, $P < 0.001$). Points, although rare, are one of the few retouched tools restricted to strata below occurrence E. The sample includes a small (length = 42.3 mm), thin (6.6 mm) bifacial point of obsidian (Fig. 1) at 160–170 cmbs in trench A, with a second quartz biface tip from 180–185 cmbs from trench C + balk. The combination of artifact types suggests that strata below occurrence E span the MSA/LSA transition, although whether this combination reflects "transitional" assemblages or a postdepositional admixture of MSA and LSA artifact-bearing strata is uncertain (*SI Text*).

The age of the deposits below occurrence E is constrained only by the >46,710 ± 3,852 ^{14}C y B.P. date from 140 to 150 cmbs in the test pit and the 25,868 ± 186 cal y B.P. date from 190 cmbs to bedrock from trench A (Table 1). This age range of ∼26 to >46 kya for the lower strata at GvJm-22 is consistent with data from similarly aged industries from sites near GvJm-22, including the Nasera and Lemuta Industries at Nasera and perhaps Mumba rock shelters in Tanzania and the Sakutiek Industry at Enkapune ya Muto in Kenya (*SI Text* and Fig. S1). All contain MSA/LSA sequences and transitional artifact industries with small Levallois cores and flakes, retouched points, an abundance of small scrapers, backed pieces ∼24 mm in length, grindstones, ochre, and OES beads (2, 4, 44–46). Pleistocene occurrences from GvJm-22, Nasera, Mumba, and Enkapune ya Muto contain obsidian from sources near Lake Naivasha at distances 100–300 km from the source (47–49). Similar archaeological sequences and shared raw material sources suggest population interconnections and extensive Late Pleistocene social networks throughout southern Kenya and northern Tanzania.

KNM-LH 1 in Context

KNM-LH 1 occurs within occurrence E at 138–140 cmbs, dates to ∼23 kya, and is the only hominin cranium found with an LGM/LSA assemblage from eastern Africa. KNM-LH 1 thus plays an important role in our understanding of the morphology of these populations. Our formal description of KNM-LH 1 extends the description of Gramly and Rightmire (29), augmented by computed tomography (CT). KNM-LH 1 preserves two-thirds of the frontal bone and most of the left parietal bone (Fig. S3). The superciliary ridges are very pronounced and joined medially by a projecting glabella that is clearly separated from the rest of the frontal bone. A sulcus separates the ridges from the robust lateral trigone [supraorbital torus grade 4 (50)]. This morphology is rare among recent modern humans (RMHs) from Africa but is well represented in our Late Pleistocene North African (LPA) sample (Table S2) where preserved (25%, $n = 67$).

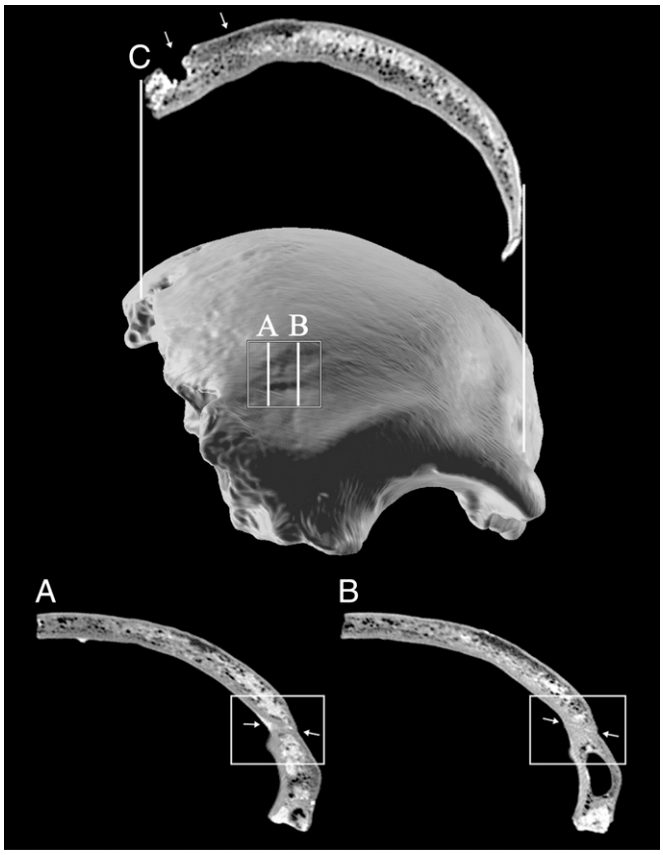

Fig. 2. Three-dimensional model of the frontal bone in anterior view, showing the healed frontal trauma and the inner structure of the frontal squama. The zone of trauma is demarcated by the white rectangle. (*A* and *B*) Two sagittal sections intersect the healed trauma, as shown by white arrows. (*C*) Coronal section is given at the level of the postmortem perforation of the right side of the frontal squama (left arrow). The right arrow outlines the pathological inner structure changes of the diploe and outer table.

The frontal bone exhibits two areas of antemortem and postmortem damage (Fig. 2). One centimeter above the glabella, a healed linear transverse trauma (10 mm in length) is present. The surrounding area (over a radius of ∼15 mm) is depressed and slightly remodeled, affecting the curvature of the frontal bone at this level. Sagittal CT sections of this portion reveal a healed complete fracture of the frontal bone without displacement, corresponding to the outer linear trauma (compare Fig. 2 *A* and *B*). The second area of damage is located 6 cm from the right orbital margin, along the broken and eroded right edge of the frontal squama. A circular perforation about 6 mm in diameter and 5 mm in depth is visible. It crosses the outer table and half of the diploe (compare Fig. 2*C*). As suggested by A. Walker (51), it might be related to a tooth mark from a carnivore.

The cranium is thick [10.2-mm thickness at the (left) parietal eminence (TPE), 10.0-mm thickness for the frontal squama]. CT images show a relatively thick vault compared with modern humans, with wide diploe and proportionate tables, with the exception of the right part of the frontal squama. In this area, the outer table seems to have thinned, the diploe is wider, and slight porosities are visible on the external surface of the bone. Nonpathological high cranial thickness is a common characteristic of Late Pleistocene *H. sapiens* that may reflect elevated activity levels compared with recent populations (52). However, the morphology of the right side of the frontal bone, with its expanded and slightly modified diploe, suggests some caution in accepting this interpretation for

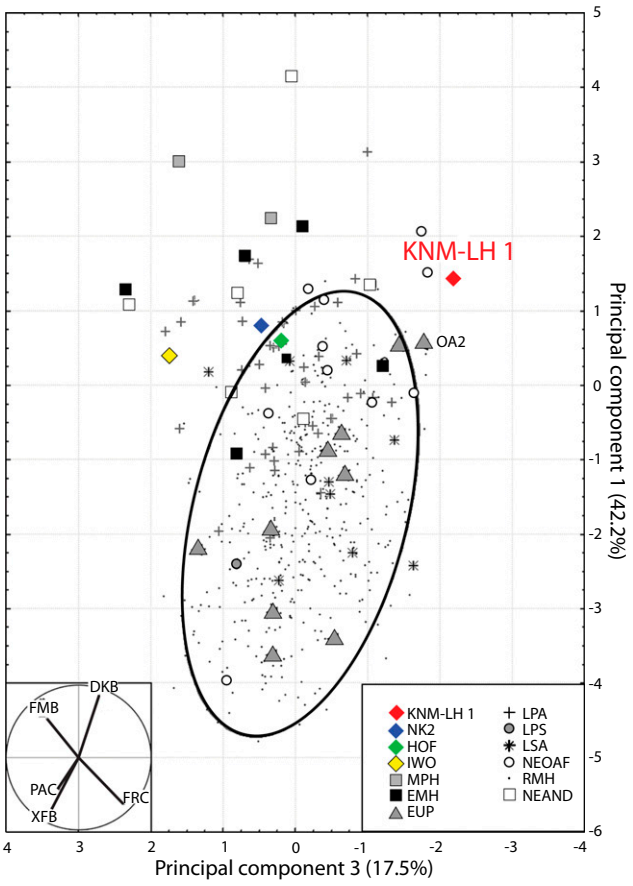

Fig. 3. Scatter plot of the first and third principal components of the principal component analysis computed on size-adjusted cranial dimensions. The ellipse represents 95% of the RMH variation. (*Inset*) Correlation circle in the lower left corner of the projection shows the position of the craniometric variables in relation to the two plotted principal components. DKB, interorbital breadth; FMB, bifrontal breadth; FRC, frontal chord; PAC, parietal chord; XFB, maximum frontal breadth. Metric data for HOF, IWO, MPH, and NEAND come from published measurements (61–66). Data for NK2, La Chapelle-aux-Saints 1, La Ferrassie 1, and Spy 1 were taken on the originals. NK2, Nazlet Khater 2; HOF, Hofmeyr; IWO, Iwo Eleru; OA2, Peştera cu Oase 2; MPH, Middle Pleistocene *Homo* fossils from Africa; EMH, early modern human fossils from Africa and Southwest Asia; EUP, European Upper Paleolithic modern human fossils; LPA, Late Pleistocene fossils or samples from North Africa; LPS, Late Pleistocene fossils or samples from Southwest Asia; LSA, Late Stone Age fossils or samples from Sub-Saharan Africa; NEOAF, Neolithic fossils or samples from North Africa; RMH, recent modern human samples; NEAND, Neandertals.

KNM-LH 1 (compare Fig. 2*C*). Although located in a small area of the calvaria and associated with no other criteria (e.g., absence of cribra orbitalia, presence of frontal sinus), this thickening, together with the external porosity, could be related to healed expression of light porotic hyperostosis (53). The alternate hypothesis for the localized porotic cranial changes on the right side of the frontal bone is that they are related to periosteal reactions resulting from trauma infection (54). In either case, the TPE does not seem to be associated with bone remodeling.

In their formal description of the specimen, Gramly and Rightmire (29) emphasized the low and receding morphology of the frontal region as being distinct from the morphology seen in modern African populations. Here, we expand the comparison of the KNM-LH 1 partial cranium to a geographically and temporally diverse sample through univariate and multivariate analyses. The comparative sample groups are listed in Table S2 and include Middle Pleistocene to Holocene individuals from Europe, Southwest Asia, and across Africa. The measurements of KNM-LH 1 were made on the 3D reconstruction of the calvaria with Avizo 7 and are given in Table S3 with the comparative ranges of variation of the early modern human (EMH), Late Pleistocene modern human (LPMH), and RMH samples. KNM-LH 1 differs from the LPMH sample in relation to its vault thickness and the morphology of the frontal bone [frontotransverse index (IFT)]. KNM-LH 1 possesses a significantly less divergent frontal squama (IFT = 92.79) than the LPMH group, lying in the EMH range of variation (IFT = 87.9 ± 3.5, n = 10; Table S3). Compared with the RMH group, KNM-LH 1 falls outside the upper limit of the RMH variation regarding its anterior frontal breadths (bifrontal breadth and interorbital breadth) and the frontal length [frontal chord (FRC)]. Focusing on calvarial shape, we performed a principal component analysis on five size-adjusted measurements (55, 56). The results are shown in Fig. 3. In terms of the shape of the calvaria, KNM-LH 1 is distinct from recent Africans and Holocene LSA samples. It is also distinct from most of the comparably aged European Upper Paleolithic (EUP) samples, except, interestingly, Peştera cu Oase, the oldest EUP cranium. Instead, KNM-LH 1 and several Late Pleistocene African crania (e.g., Nazlet Khater 2, Iwo Eleru, the LPA group) fall outside of the RMH variation along the first axis. The separation along the first axis is related to the combination of large anterior frontal breadths in relation to the maximal frontal breadth and the FRC. The separation of KNM-LH 1 along the third axis is related to its relatively great frontal length.

Unlike face or basicranial shape, neurocranial shape is generally considered a useful measure of population history (57, 58). Our results emphasize distinct temporal and spatial differences in cranial shape among modern humans (*H. sapiens*). KNM-LH 1 and other Pleistocene African specimens, all of which are potentially sampling candidate populations for dispersals across and out of Africa during the Late Pleistocene (12–15, 50, 59), differ substantially not only from recent Africans but also from individuals drawn from Holocene LSA archaeological sites. KNM-LH 1 and other Pleistocene African specimens (found with MSA and LSA artifacts) are also distinct from most EUP individuals. The limited similarity between the Late Pleistocene African and European samples indicates that KNM-LH 1 samples elements of modern human variability not found in current lineages and attests to the still poorly understood interactions between demography, dispersals, behavior, and climate that have shaped human cranial variation over the past >70,000 y (60).

Conclusions

Renewed chronometric, lithic technological, and morphological analyses of the hominin partial cranium (KNM-LH 1) from site GvJm-22 at Lukenya Hill demonstrate (*i*) a Last Glacial Maximum age for KNM-LH 1, (*ii*) an extended age range for archaeological deposits at the site to >46,710 ± 3,852 ^{14}C y B.P., (*iii*) the presence of lithic artifacts typically associated with MSA or transitional MSA/LSA industries in deposits underlying KNM-LH 1, and (*iv*) the substantial and still poorly documented variability among aspects of cranial shape among Late Pleistocene *H. sapiens* across Africa and Eurasia. Although the record of MSA and LSA sites and hominin remains in eastern Africa is sparse and discovery of additional sites through further fieldwork is badly needed (46), our reexamination of the 1970–1973 collections from GvJm-22 at Lukenya Hill show the value of a critical analysis of museum collections for understanding the behavior and biology of Late Pleistocene *H. sapiens*.

Materials and Methods

All archaeological materials (including OES fragments) were studied and sampled from collections curated at the NMK in Nairobi. Comparisons of artifact dimensions used an unequal variance t test, unless otherwise specified. Analyses of the KNM-LH 1 hominin cranial fragments (also stored at the NMK) were augmented by CT scans made with a Siemens Sensation 16 scanner. The three fragments were oriented perpendicular to the scan plane to give optimal visualization of the tables and diploe, using a slice spacing of 0.3 mm and a pixel size of 0.23 mm.

ACKNOWLEDGMENTS. We thank Drs. Greg Hodgins, Pierre Guyomarc'h, Alex Tokovinine, Christine Lane, Warren Sharp, and Linda Reynard for advice and assistance, and particularly R. M. Gramly for his continued support throughout this project. Sheila Nightingale provided the excellent artifact illustrations. We thank the following institutions and persons for providing permission to study the comparative material and the CT scan data: The British Museum (N. Spencer, D. Antoine), University of Colorado Boulder (D. Van Gerven), Institut de Paléontologie Humaine (H. de Lumley, D. Grimaud-Hervé), Laténium (M. Honegger), Muséum national d'Histoire naturelle (Ph. Mennecier), NMK, National Museum of Natural History (Smithsonian Institution; D. Hunt), Royal Belgian Institute of Natural Sciences (P. Semal), and Staatssammlung für Anthropologie und Paläoanatomie (G. McGlynn). This research was conducted under Research Permit NCST/5/002/R/576 issued to C.A.T. by the Government of the Republic of Kenya while an affiliate of the NMK and was supported by funds from the American School for Prehistoric Research and Harvard University.

1. Mitchell P (1996) Prehistoric exchange and interaction in southeastern southern Africa: Marine shells and ostrich eggshell. *African Archaeological Review* 13(1):35–76.
2. Ambrose SH (1998) Chronology of the Later Stone Age and Food Production in East Africa. *J Archaeol Sci* 25(4):377–392.
3. Ambrose SH (2001) Middle and Later Stone Age settlement patterns in the central Rift Valley, Kenya: Comparisons and contrasts. *Settlement Dynamics of the Middle Paleolithic and Middle Stone Age*, ed Conard N (Kerns, Tubingen, Germany), pp 21–43.
4. Ambrose SH (2002) Small things remembered: Origins of early microlithic industries in sub-Saharan Africa. *Thinking Small: Global Perspectives on Microlithization*, Archaeological Papers of the American Anthropological Association No. 12, eds Elston RG, Kuhn SL (American Anthropological Association, Washington, DC), pp 9–29.
5. Deacon HJ, Deacon J (1999) *Human Beginnings in South Africa: Uncovering the Secrets of the Stone Age* (Altamira Press, Claremont, CA).
6. Barham L, Mitchell P (2008) *The First Africans: African Archaeology from the Earliest Toolmakers to Most Recent Foragers* (Cambridge Univ Press, Cambridge, UK).
7. Faith JT (2008) Eland, buffalo, and wild pigs: Were Middle Stone Age humans ineffective hunters? *J Hum Evol* 55(1):24–36.
8. d'Errico F, et al. (2012) Early evidence of San material culture represented by organic artifacts from Border Cave, South Africa. *Proc Natl Acad Sci USA* 109(33):13214–13219.
9. Villa P, et al. (2012) Border Cave and the beginning of the Later Stone Age in South Africa. *Proc Natl Acad Sci USA* 109(33):13208–13213.
10. Prugnolle F, Manica A, Balloux F (2005) Geography predicts neutral genetic diversity of human populations. *Curr Biol* 15(5):R159–R160.
11. von Cramon-Taubadel N, Lycett SJ (2008) Brief communication: Human cranial variation fits iterative founder effect model with African origin. *Am J Phys Anthropol* 136(1):108–113.
12. Crevecoeur I, Rougier H, Grine F, Froment A (2009) Modern human cranial diversity in the Late Pleistocene of Africa and Eurasia: Evidence from Nazlet Khater, Peştera cu Oase, and Hofmeyr. *Am J Phys Anthropol* 140(2):347–358.
13. Gunz P, et al. (2009) Early modern human diversity suggests subdivided population structure and a complex out-of-Africa scenario. *Proc Natl Acad Sci USA* 106(15): 6094–6098.
14. Rito T, et al. (2013) The first modern human dispersals across Africa. *PLoS ONE* 8(11): e80031.
15. Soares P, et al. (2012) The Expansion of mtDNA Haplogroup L3 within and out of Africa. *Mol Biol Evol* 29(3):915–927.
16. Vallois HV (1951) La mandibule humaine fossile de la Grotte du Porc-Epic près Diré-Daoua (Abyssinie). *Anthropologie* 55:231–238. French.
17. Willoughby PR (2012) The Middle and Later Stone Age in the Iringa Region of southern Tanzania. *Quat Int* 270:103–118.
18. Pleurdeau D, et al. Cultural change or continuity in the late MSA/Early LSA of southeastern Ethiopia? The site of Goda Buticha, Dire Dawa area. *Quat Int* 343:117–135.
19. Clark PU, et al. (2009) The Last Glacial Maximum. *Science* 325(5941):710–714.
20. Gramly RM (1976) Upper Pleistocene archaeological occurrences at site GvJm/22, Lukenya Hill, Kenya. *Man (Lond)* 11:319–344.
21. Marean CW (1992) Implications of late Quaternary mammalian fauna from Lukenya Hill (south-central Kenya) for paleoenvironmental change and faunal extinctions. *Quaternary Research* 37:239–255.
22. Merrick HV (1975) Change in Later Pleistocene lithic industries in eastern Africa. PhD dissertation (University of California, Berkeley, CA).
23. Barut S (1997) Later Stone Age lithic raw material use at Lukenya Hill, Kenya. PhD dissertation (University of Illinois at Urbana–Champaign, Champaign, IL).
24. Reimer PJ, et al. (2013) IntCal13 and Marine13 radiocarbon age calibration curves 0–50,000 years cal BP. *Radiocarbon* 55(4):1869–1887.
25. Gramly RM (1975) Pastoralists and hunters: Recent prehistory in southern Kenya and northern Tanzania. PhD dissertation (Harvard University, Cambridge, MA).
26. Wilshaw A (2012) An investigation into the LSA of the Nakuru-Naivasha Basin and Surround, Central Rift Valley, Kenya: Technological classifications and population considerations. PhD dissertation (Cambridge University, Cambridge, UK).
27. Faith JT, et al. (2012) New perspectives on middle Pleistocene change in the large mammal faunas of East Africa: *Damaliscus hypsodon* sp. nov. (Mammalia, Artiodactyla) from Lainyamok, Kenya. *Palaeogeogr Palaeoclimatol Palaeoecol* 361–362:84–93.
28. Faith JT, Tryon CA, Peppe DJ, Fox DL (2013) The fossil history of Grevy's zebra (*Equus grevyi*) in Equatorial East Africa. *J Biogeogr* 40:359–369.
29. Gramly RM, Rightmire GP (1973) A fragmentary cranium and dated Later Stone Age assemblage from Lukenya Hill, Kenya. *Man (Lond)* 8:571–579.
30. Collett D, Robertshaw P (1983) Problems in the interpretation of radiocarbon dates: The Pastoral Neolithic of East Africa. *African Archaeological Review* 1:57–74.
31. Ambrose SH (1990) Preparation and characterization of bone and tooth collagen for isotopic analysis. *J Archaeol Sci* 17:431–451.
32. Marean CW (1990) Late Quaternary paleoenvironments and faunal exploitation in East Africa. PhD dissertation (University of California, Berkeley, CA).
33. Higham TFG, Jacobi RM, Bronk Ramsey C (2006) AMS radiocarbon dating of ancient bone using ultrafiltration. *Radiocarbon* 48(2):179–195.
34. Longin R (1971) New method of collagen extraction for radiocarbon dating. *Nature* 230(5291):241–242.
35. Long A, Hendershott RB, Martin PS (1983) Radiocarbon dating of fossil eggshell. *Radiocarbon* 25(2):533–539.
36. Freundlich JC, Kuper R, Breunig P, Bertram H-G (1989) Radiocarbon dating of ostrich eggshells. *Radiocarbon* 31(3):1030–1034.
37. Janz L, Elston RG, Burr GS (2009) Dating North Asian surface assemblages with ostrich eggshell: Implications for paleoecology and extirpation. *J Archaeol Sci* 36(9):1982–1989.
38. Vogel JC, Visser E, Fuls A (2001) Suitability of ostrich eggshell for radiocarbon dating. *Radiocarbon* 43(1):133–137.
39. Bronk Ramsey C (2009) Bayesian analysis of radiocarbon dates. *Radiocarbon* 51(1): 337–360.
40. Smith MA (1986) The antiquity of seedgrinding in arid Australia. *Archaeology in Oceania* 21(1):29–39.
41. Smith MA (1988) Central Australian seed grinding implements and Pleistocene grindstones. *Archaeology with Ethnography: An Australian Perspective*, eds Meehan B, Jones R (Department of Prehistory, Research School of Pacific Studies, The Australian National University, Canberra, Australia), pp 94–108.
42. Boëda É (1994) *Le concept Levallois: Variabilité des méthodes* (Centre National de la Recherche Scientifique Éditions, Paris). French.
43. Yellen J, et al. (2005) The archaeology of Aduma Middle Stone Age sites in the Awash Valley, Ethiopia. *Paleoanthropology* 2005:25–100.
44. Mehlman MJ (1989) Late Quaternary archaeological sequences in northern Tanzania. PhD dissertation (University of Illinois at Urbana–Champaign, Champaign, IL).
45. Gliganic LA, Jacobs Z, Roberts RG, Domínguez-Rodrigo M, Mabulla AZP (2012) New ages for Middle and Later Stone Age deposits at Mumba rockshelter, Tanzania: Optically stimulated luminescence dating of quartz and feldspar grains. *J Hum Evol* 62(4):533–547.
46. Tryon CA, Faith JT (2013) Variability in the Middle Stone Age of Eastern Africa. *Curr Anthropol* 54(Suppl 8):S234–S254.
47. Brown FH, Nash BP, Fernandez DP, Merrick HV, Thomas RJ (2013) Geochemical composition of source obsidians from Kenya. *J Archaeol Sci* 40(8):3233–3251.
48. Merrick HV, Brown FH (1984) Obsidian sources and patterns of source utilization in Kenya and northern Tanzania: Some initial findings. *African Archaeological Review* 2(1):129–152.
49. Merrick HV, Brown FH, Nash WP (1994) Use and movement of obsidian in the Early and Middle Stone Ages of Kenya and northern Tanzania. *Society, Culture, and Technology in Africa*, ed Childs ST (Museum Applied Science Center for Archaeology, Philadelphia), pp 29–44.
50. Lahr MM, Foley RA (1998) Towards a theory of modern human origins: Geography, demography, and diversity in recent human evolution. *Yearb Phys Anthropol* 41:137–176.
51. Gramly RM (1971) *Recent Archaeological Survey in Central Kenya*. University of Nairobi Institute of African Studies Discussion Paper No. 19 (University of Nairobi Institute of African Studies, Nairobi, Kenya), pp 1–18.
52. Lieberman DE (1996) How and why humans grow thin skulls: Experimental evidence for systemic cortical robusticity. *Am J Phys Anthropol* 101(2):217–236.
53. Stuart-Macadam P (1987) A radiographic study of porotic hyperostosis. *Am J Phys Anthropol* 74(4):511–520.
54. Ortner DJ (2003) *Identification of Pathological Conditions in Human Skeletal Remains* (Academic, London), 2nd Ed.
55. Darroch JN, Mosimann JE (1985) Canonical and principal components of shape. *Biometrika* 72(2):241–252.
56. Jungers WL, Falsetti AB, Wall CE (1995) Shape, relative size, and size-adjustments in morphometrics. *Yearb Phys Anthropol* 38(S21):137–161.
57. Lieberman DE, McBratney BM, Krovitz G (2002) The evolution and development of cranial form in *Homo sapiens*. *Proc Natl Acad Sci USA* 99(3):1134–1139.
58. Harvati K, Weaver TD (2006) Human cranial anatomy and the differential preservation of population history and climate signatures. *Anat Rec A Discov Mol Cell Evol Biol* 288(12):1225–1233.
59. Stojanowski CM (2014) Iwo Eleru's place among Late Pleistocene and Early Holocene populations of North and East Africa. *J Hum Evol* 75:80–89.
60. Pearson O (2013) Hominin evolution in the Middle-Late Pleistocene: Fossils, adaptive scenarios, and alternatives. *Curr Anthropol* 54(Suppl 8):S221–S233.
61. Bräuer G, Leakey RE (1986) A new archaic *Homo sapiens* cranium from Eliye Springs, West Turkana, Kenya. *Z Morphol Anthropol* 76(3):245–252.
62. Grine FE, Gunz P, Betti-Nash L, Neubauer S, Morris AG (2010) Reconstruction of the late Pleistocene human skull from Hofmeyr, South Africa. *J Hum Evol* 59(1):1–15.
63. Hublin J-J (1991) L'émergence des *Homo sapiens* archaïques: Afrique du Nord-Ouest et Europe occidentale. Thèse d'Etat (Université Bordeaux 1, Bordeaux, France). French.
64. Magori CC, Day MH (1983) An early *Homo sapiens* skull from the Ngaloba Beds, Laetoli, Northern Tanzania. *Anthropos* 10:143–183.
65. Trinkaus E (1983) *The Shanidar Neandertals* (Academic, London).
66. Vandermeersch B (1981) *Les Hommes Fossiles de Qafzeh (Israël)* (Éditions CNRS, Paris). French.